Supplementary Information for

Recent giant detachment of a glacier in Tibet provoked by its frozen tongue

Andreas Kääb *et al.*

*Corresponding author. Email: kaeaeb@geo.uio.no

This PDF file includes:

Tab. S1 and S2, and Fig. S1 to S13

Tab. S1 Specifications of geographic data.

Key specifications of most important geographic data used. DEM: digital elevation model. HMA: High-mountain Asia. n/a: not applicable. *: nominal, from product specifications.

Data set (time)	Ground sampling distance	Horizontal accuracy	Vertical accuracy	Comment
External sources				
PlanetScope optical satellite images (diverse times)	3 m	~2–3 m after co-registration	n/a	Orthorectified; used for glacier velocities after co-registration, and visual interpretation
Sentinel-2 optical satellite images (diverse times)	10 m	~2–3 m after co-registration	n/a	Orthorectified; used for glacier velocities after co-registration, and visual interpretation
Very-high resolution optical images; WorldView, Pléiades, SPOT6 (diverse times)	0.5–6 m	~60 cm RMS (against GoogleEarth), if relevant	n/a	Partially orthorectified, partially for visual interpretation only
ASTER nighttime thermal infrared (May 2021)	90 m	not relevant	n/a	Orthorectified; used for visual interpretation
Copernicus DEM (2011-2012)	0.00028° (~28m)	< 6 m (circular error, 90% confidence)*	~2–4m (mean absolute accuracy), >96% (relative accuracy)* ~2m (stable ground std.dev. against HMA DEM after vertical co-registration) ~ 0.5–1m (stable ground std.dev. against ICESat-2 after vertical co-registration)	Vertical bias removed for elevation differences
HMA optical stereo DEM (Jan 2015)	8 m	< 5 m (circular error, 90% confidence)*	~2m (stable ground std.dev. against Copernicus DEM after vertical co-registration) ~ 0.5–1m (stable ground std.dev. against ICESat-2 after vertical co-registration)	Vertical bias removed for elevation differences
ICESat-2 satellite laser altimetry (diverse times)	70 cm (single photons), 40m (ATL06 product); profile	~6.5 m (1σ)*	< 10cm* ~ 0.5–1m (stable ground std.dev. against Copernicus DEM and HMA DEM after vertical co-registration)	Vertical bias removed for elevation differences
Other geographic data used for interpretation: Corona satellite photos; Landsat images; Sentinel-1 data; SRTM DEM; TanDEM-X topographic change product				
Generated in this study				
Post-event DEM from WorldView optical satellite stereo (Jan 2023)	5 m	~60 cm RMS (against GoogleEarth)	~3m (stable ground std.dev. against Copernicus DEM after vertical co-registration) ~ 1.5 m (stable ground std.dev. against ICESat-2 after vertical co-registration)	Vertical bias removed for elevation differences
Post-event WorldView orthoimage (Jan 2023)	0.5 m (pan), 2 m (multispectral)	~60 cm RMS (against GoogleEarth)	n/a	Used for visual interpretation
Horizontal ice velocities from optical offset tracking (diverse times)	~ 100 m along centreline profile	~10 m/year	n/a	

Tab. S2 Parameters for avalanche model.

Input parameters in RAMMS::RockIce for the model run with the best fit between simulated and actual avalanche extent. Only parameters deviating from the default values of the program are given.

Release properties	Volumetric ice	1
	Temperature of the ice	−2°C
	Release depth	78 m
Field site conditions	Air temperature	−18°C
Friction parameters	Coloumb friction ice	0.05
	Turbulent coefficient	1000 m/s^2
Erosion for the flat lake shore (sediments in the lake)	Erosion rate	0.013 (0.050) m/s
	Potential erosion depth	0.05 (0.20) 1/kPa
	Critical shear stress	1.5 (0.5) kPa
	Maximum erosion depth	5 (5) m
	Volumetric soil	0.7 (0.5)
	Volumetric ice	0.2 (0)
	Volumetric water	0.1 (0.5)
	Temperature	0 (0) °C

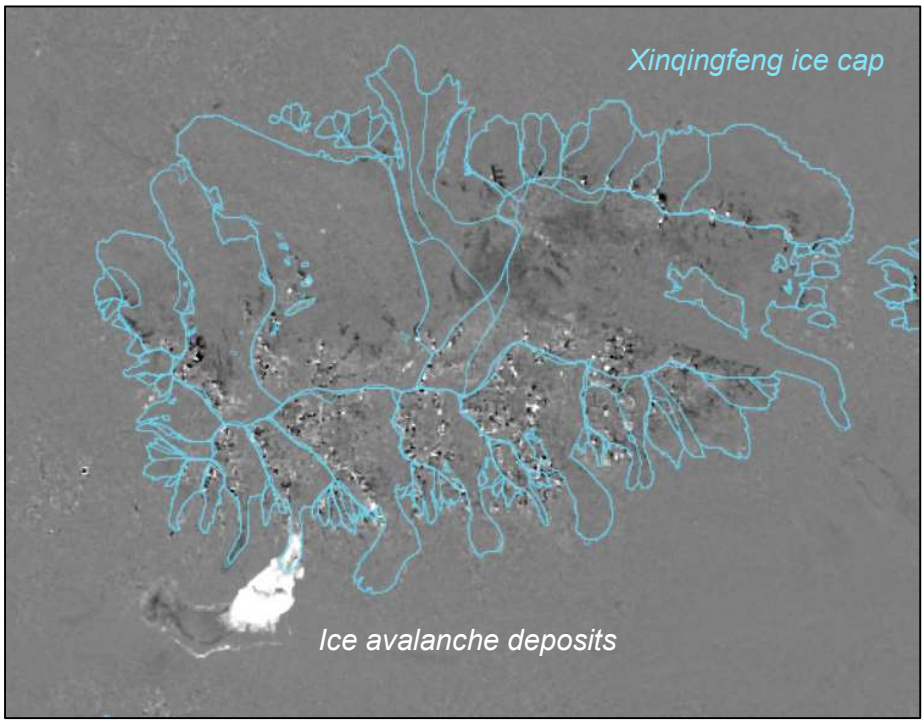

Fig. S1. Radar backscatter changes.

Sentinel-1 satellite radar backscatter changes between winter 2021/22 and 2022/23. The bright area to the lower left indicates enhanced backscatter between both winters caused by the Bukadaban East ice avalanche. The bright lake outlines left of the avalanche deposits indicate lake ice that was crushed onto the lake shore by the avalanche impact wave. The blue outlines are the Global Land Ice Measurements from Space (GLIMS) glacier outlines.

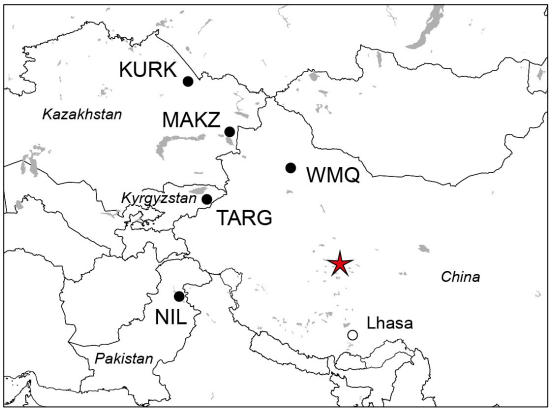

Fig. S2. Seismic stations used for initial estimate of event timing.

Location of seismic stations that recorded signals of the Bukadaban ice avalanche (cf. main text Fig. 1e). Station names are the IRIS catalogue station codes. Location of the epicentre at the Xinqingfeng ice cap indicated by a red star. Country boundaries in black. Lakes in grey shade. Data from the station in Lhasa were not available for the event time.

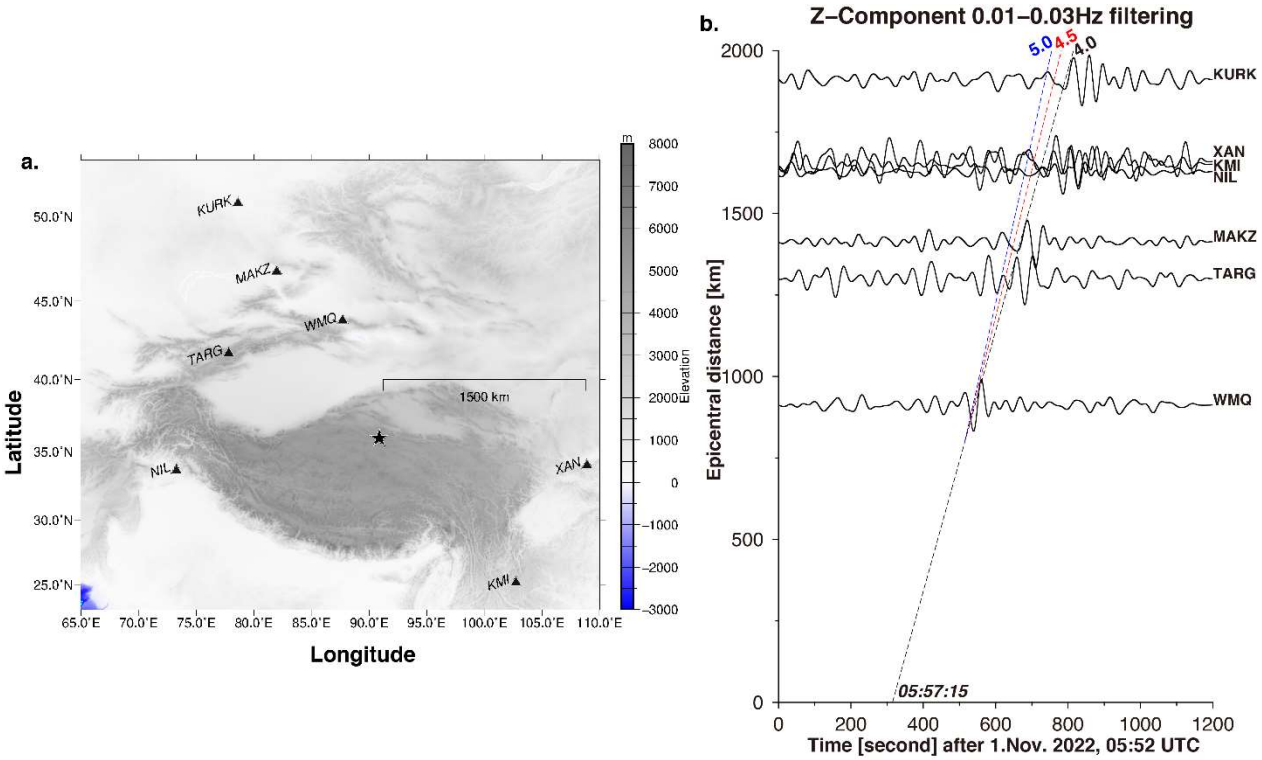

Fig. S3. Seismic stations for detailed analysis and estimate of event timing.

a, Distributions of seismic stations used in this study for detailed analysis of seismic signals (triangles) and the glacier collapse (star; 90.87°E, 35.97°N). **b**, Plots of filtered velocity seismograms in the vertical component versus epicentral distances for the event. The slope of the dashed line indicates propagation speed of 4 km/s (black), 4.5 km/s (red) and 5 km/s (blue), respectively.

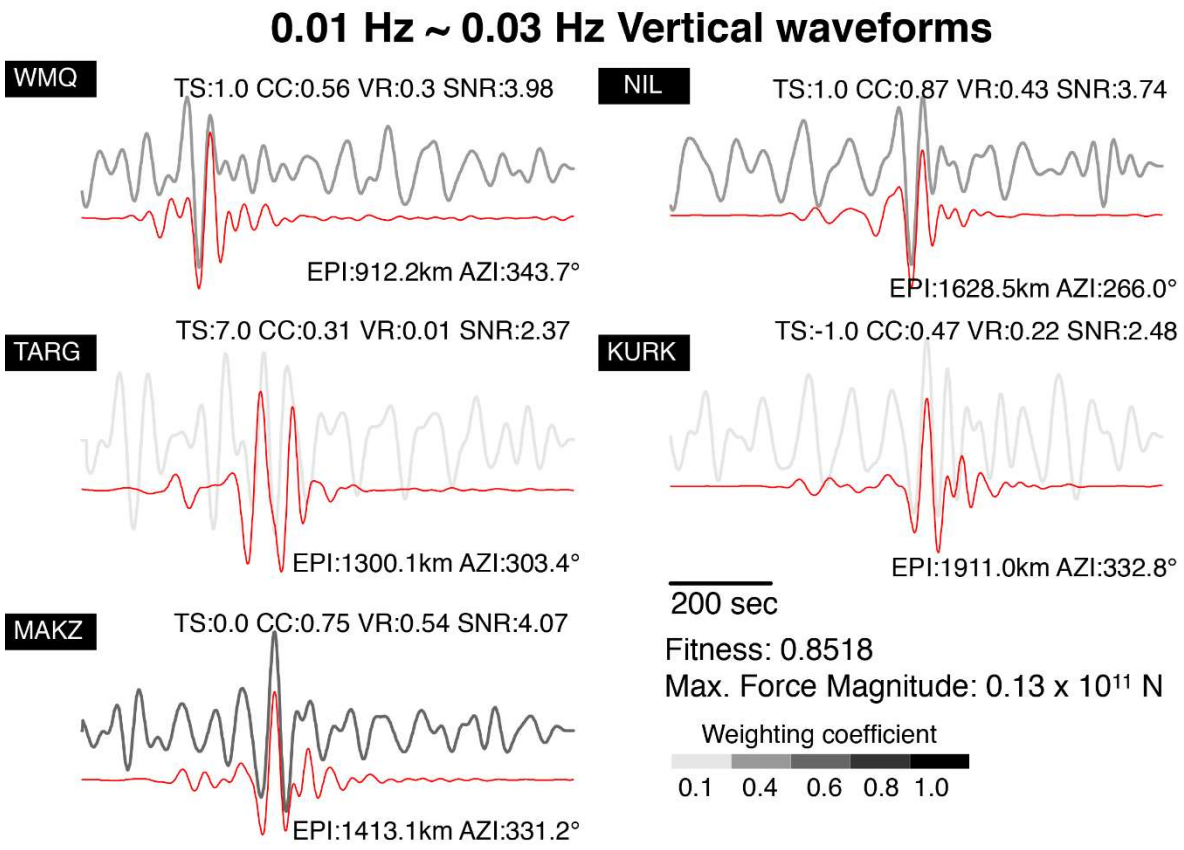

Fig. S4. Result of force-time history (LFH) inversion for the collapse event.

Traces display observed records (grey curves) and synthetic filtered (0.01–0.03 Hz) displacement seismograms calculated for the best LFH solution (shown in Fig. S5a). Different grey levels indicate different weighting coefficients based on signal-to-noise ratios (SNR) of individual records. The station name, SNR value, time shift (TS), normalized cross-correlation coefficient (CC) and variance reduction (VR) are given at the top of each trace. The epicentral distance (EPI) and station azimuth (AZI) are given at the bottom.

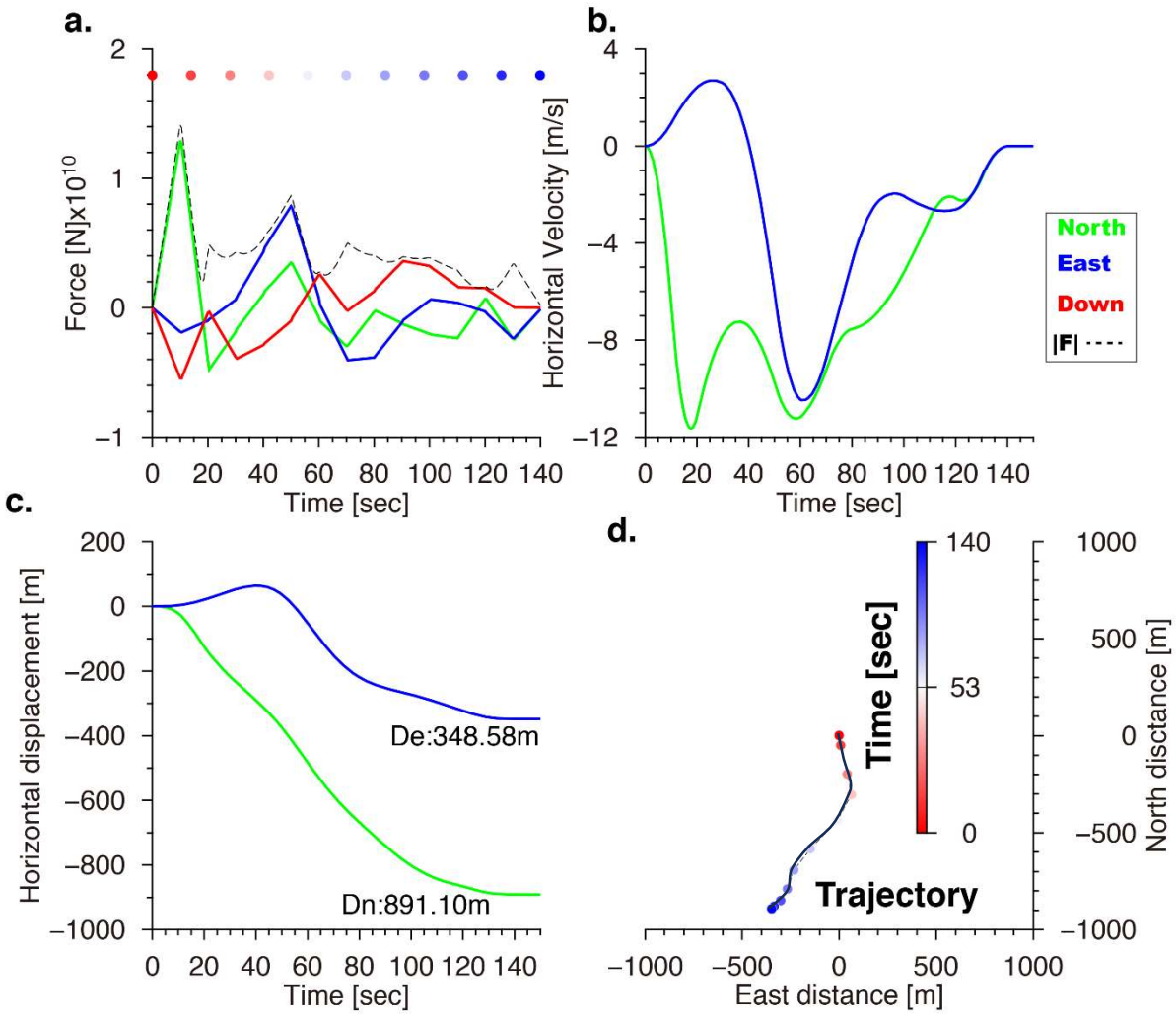

74

76 **Fig. S5. Force-time history and trajectory**

a, Force-time history (LFH) of each component (green: north; blue: east; red: down) for the
78 collapse event. Color dots and scale correspond to the time progression from 0 to 140 s in the LFH results. With a mass (m) of 0.1×10^{11} kg, three-component velocity (**b**) and displacement
80 (**c**) can be directly computed. **d**, Locations of the centre of a collapsed mass block along the run-out path trajectory (see also Fig. S10).

82

84

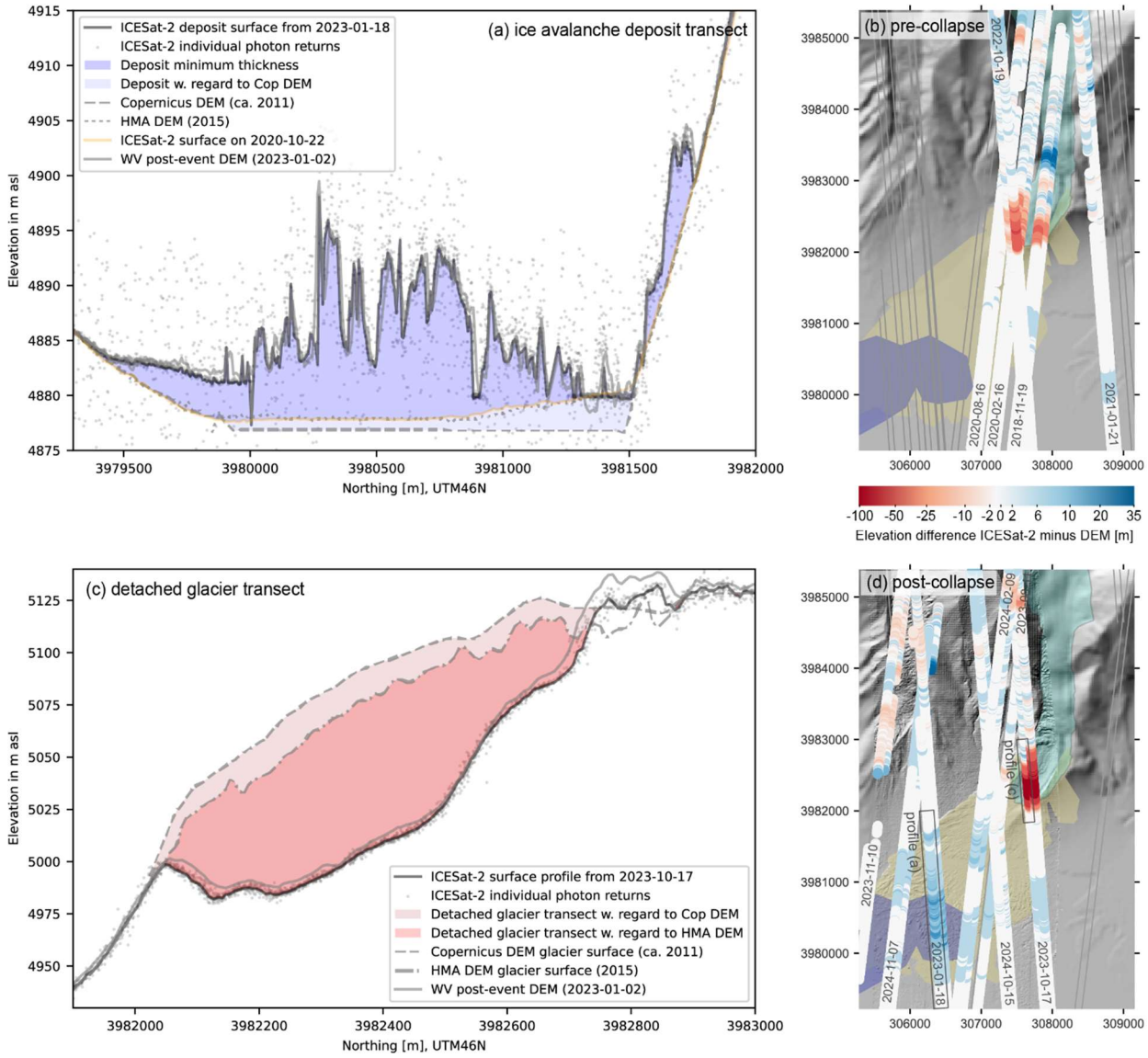

Fig. S6. Post-detachment ICESat-2 tracks of avalanche deposits and detachment. **a**, ICESat-2 elevation profile of 18 Jan 2023 (beam pair 3, weak beam) across the ice avalanche deposits and lake. Grey dots indicate ICESat-2 single photon returns that are averaged to 7m bins (black line), with corresponding pre-event DEM elevations (stippled lines). The orange line is an elevation profile from a pre-event ICESat-2 overpass along the same profile. The blue areas show the deposit thickness with regard to the pre-event reference DEM elevation (not considering erosion). The location of the profile is shown in panel (d). **b**, ICESat-2 tracks crossing the glacier prior to the detachment (2018–2022), colours indicate the elevation difference to the Copernicus DEM (from 2011–2012). The location of ICESat-2 overpasses in the same period is shown in grey. Approximate pre-event glacier/lake areas and avalanche deposit extent are shown in cyan, blue and yellow, respectively. **c**, ICESat-2 elevation profile of 17 Oct 2023 (beam pair 3, strong beam) across the detached glacier/glacier bed. Legend as in (a), with reference DEM elevations showing the glacier surface prior to detachment. **d**, ICESat-2 profile locations from after the detachment/avalanche, legend as in (b). Black boxes indicate the locations of transects (a) and (c). HMA: High Mountain Asia, WV: WorldView satellite.

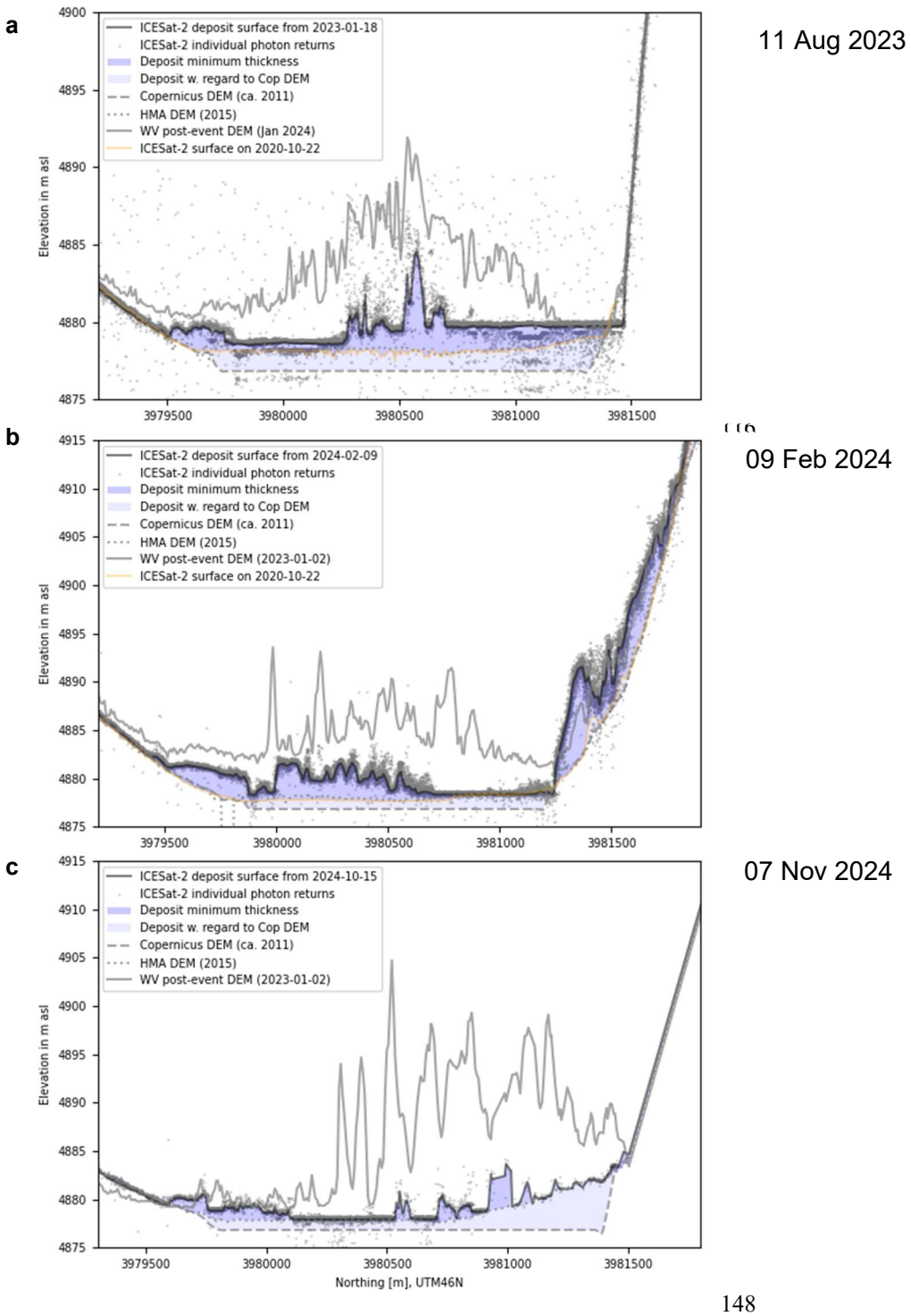

Fig. S7. Post-detachment ICESat-2 tracks of avalanche deposit melt.

ICESat-2 profiles similar to the ones in Fig. S3, but later after detachment date in order to illustrate the melt of the ice avalanche deposits. For profile locations see Fig. S6d. **a**, 11 Aug 2023. **b**, 9 Feb 2024. Note, the deposits on the slope to the right are from the smaller Oct 2023 ice avalanche after the main detachment event. **c**, 17 Nov 2024.

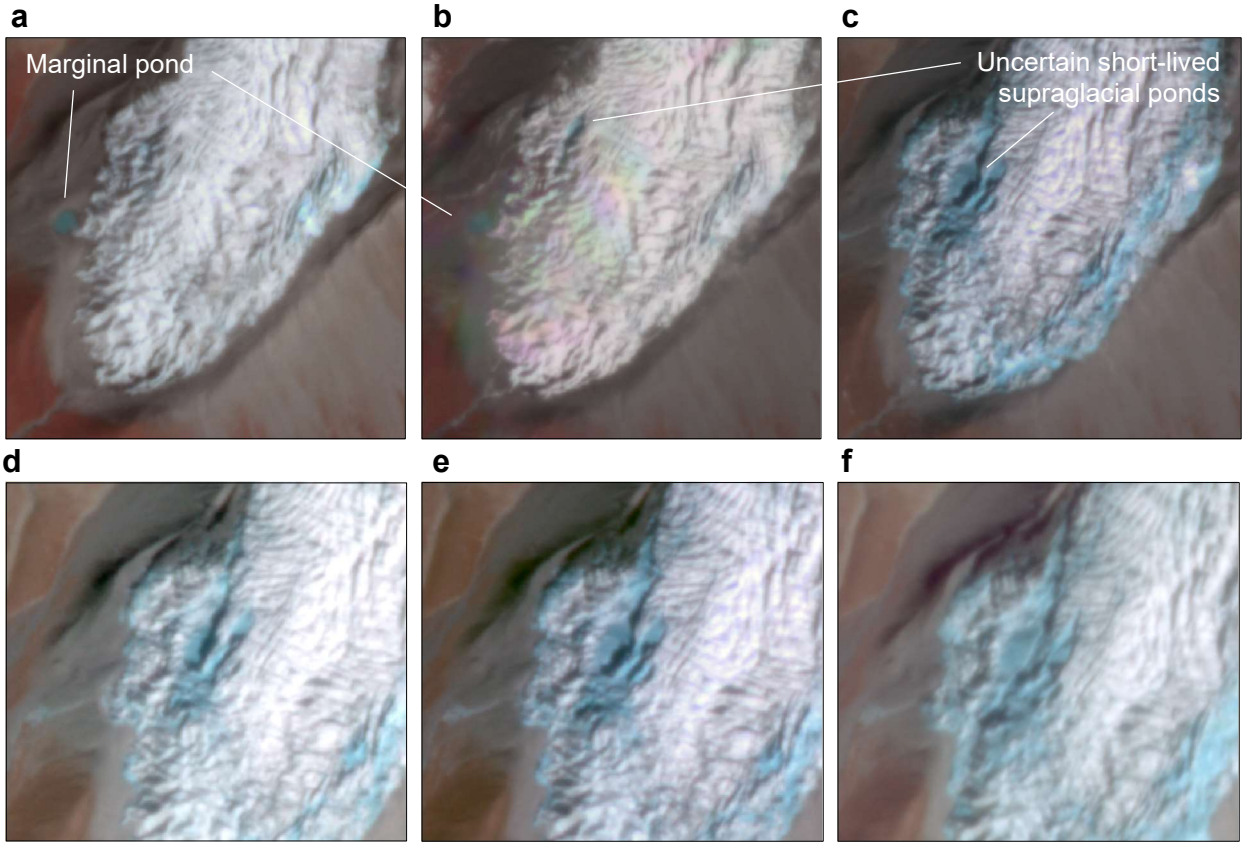

Fig. S8. Glacier tongue.

PlanetScope images of the Bukadaban East glacier tongue. **a**, 8 Oct 2022, **b**, 10 Oct 2022, **c**, 31 Oct 2022. **a** and **b** show a small ice-marginal lake to the west, which is destroyed by advancing ice in panel **c**. **b** and **c** show flat surfaces on the ice that could be, likely frozen, supraglacial ponds, but also toppled ice lamella or fans of fine ice debris. **e–f** are close-ups of 30.10., 31.10., and 1.11., respectively.

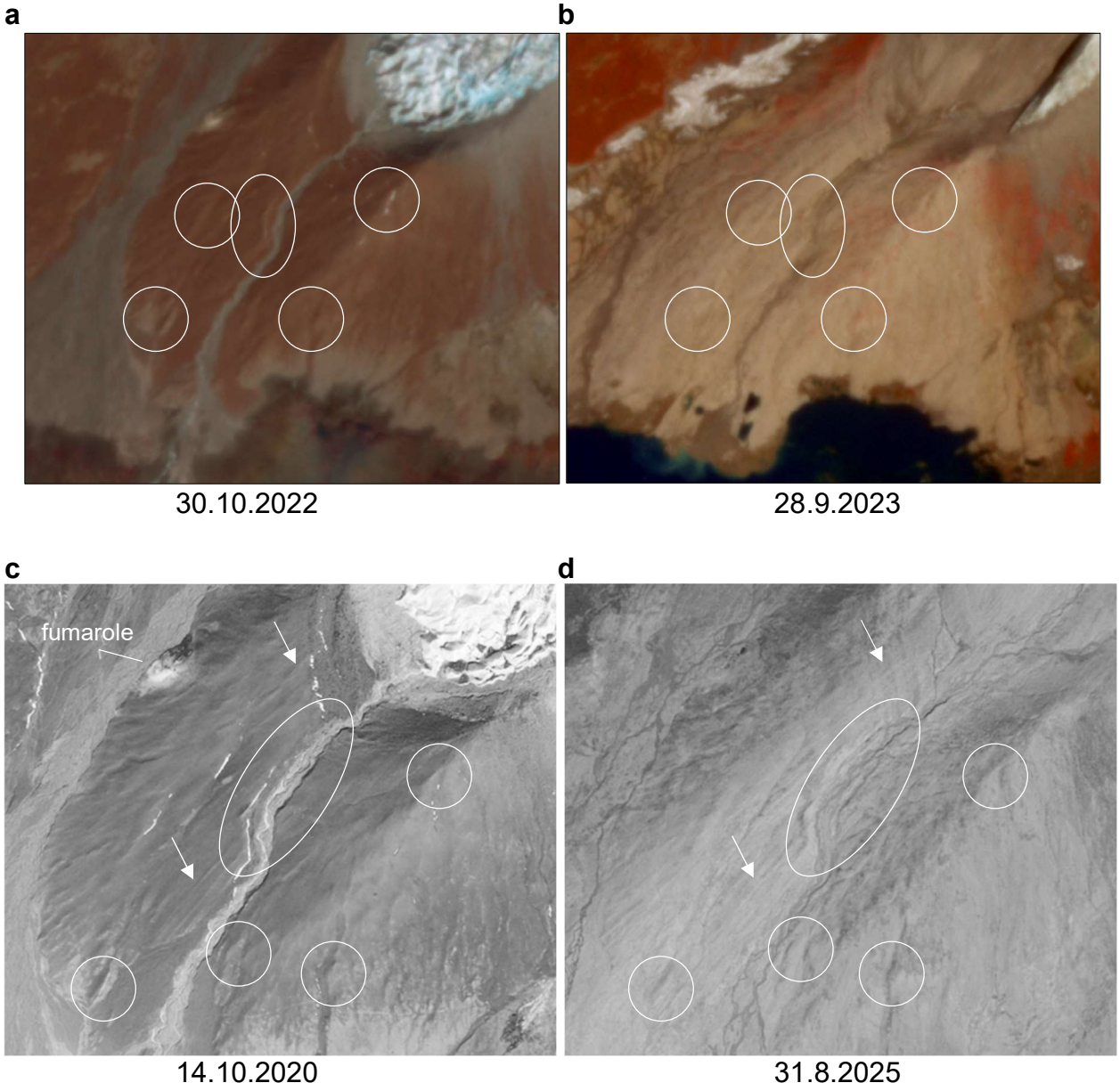

Fig. S9. Surface changes.

a, PlanetScope image of 30 Oct 2022. **b**, PlanetScope image of 28 Sep 2023. **c**, Pléiades image 14.10.2020 (courtesy Google Earth/Airbus). **d**, SPOT6 image 31.8.2025 (courtesy Airbus). White outlines mark some example areas where the surface topography was little changed through the passing avalanche, pointing to very limited erosion and sediment uptake at the base of the avalanche. Close observation shows such similarities over time at many more places over the gentle slope below the pre-event glacier terminus. The white arrows in **c** and **d** indicate two areas with ridges/stripes in glacier flow or avalanche direction. The location of the fumarole is also indicated in **c**.

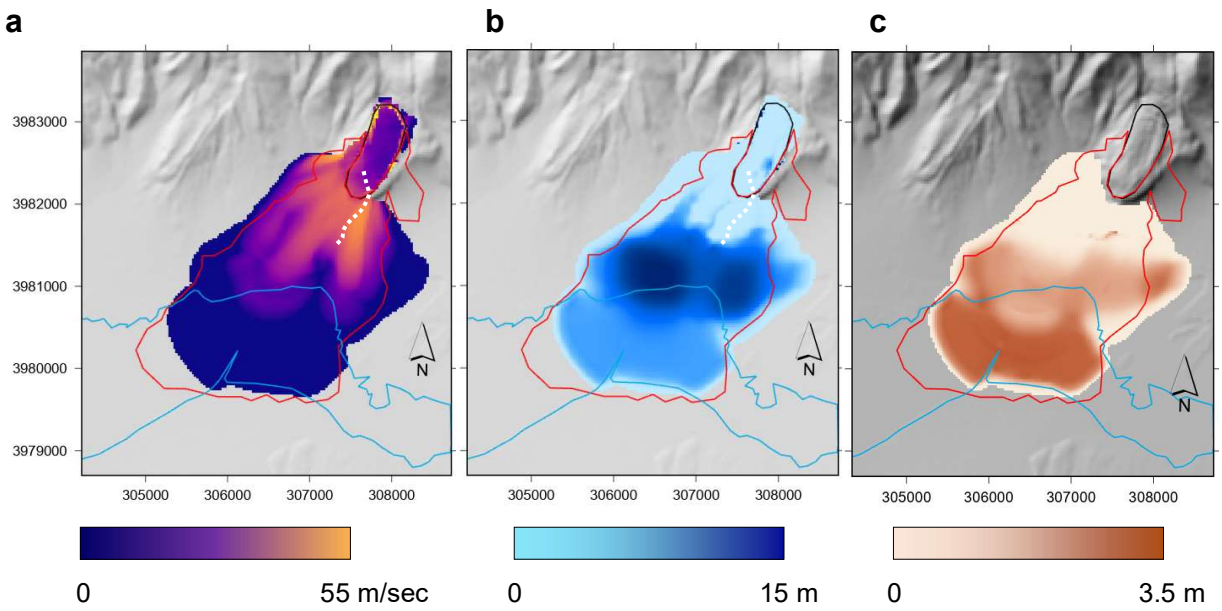

Fig. S10. Ice avalanche simulation.

a, maximum speed simulated by the RAMMS::Rock/Ice model for a parametrisation that well fits the actual avalanche deposit outlines (red). Maximum model speeds 55 m/sec (200 km/h). **b**, deposit height simulated by same model run as in panel **a**. Deposit thickness is up to 15 m. Lake outlines before the event: blue; outlines of detached glacier part: black. **c**, deposition height of the eroded sediment component simulated by same model run as in panel **a**. Maximum column average sediment height is 3.5 m. Sediments stem mostly from the easily erodible lake area. The white dashed line in **a** and **b** is the trajectory reconstructed by seismic inversion (Fig. S5d). Note, the seismic inversion does not fix the absolute position of the trajectory but it is prescribed, and its location in panels **a** and **b** is thus mainly for scale comparison.

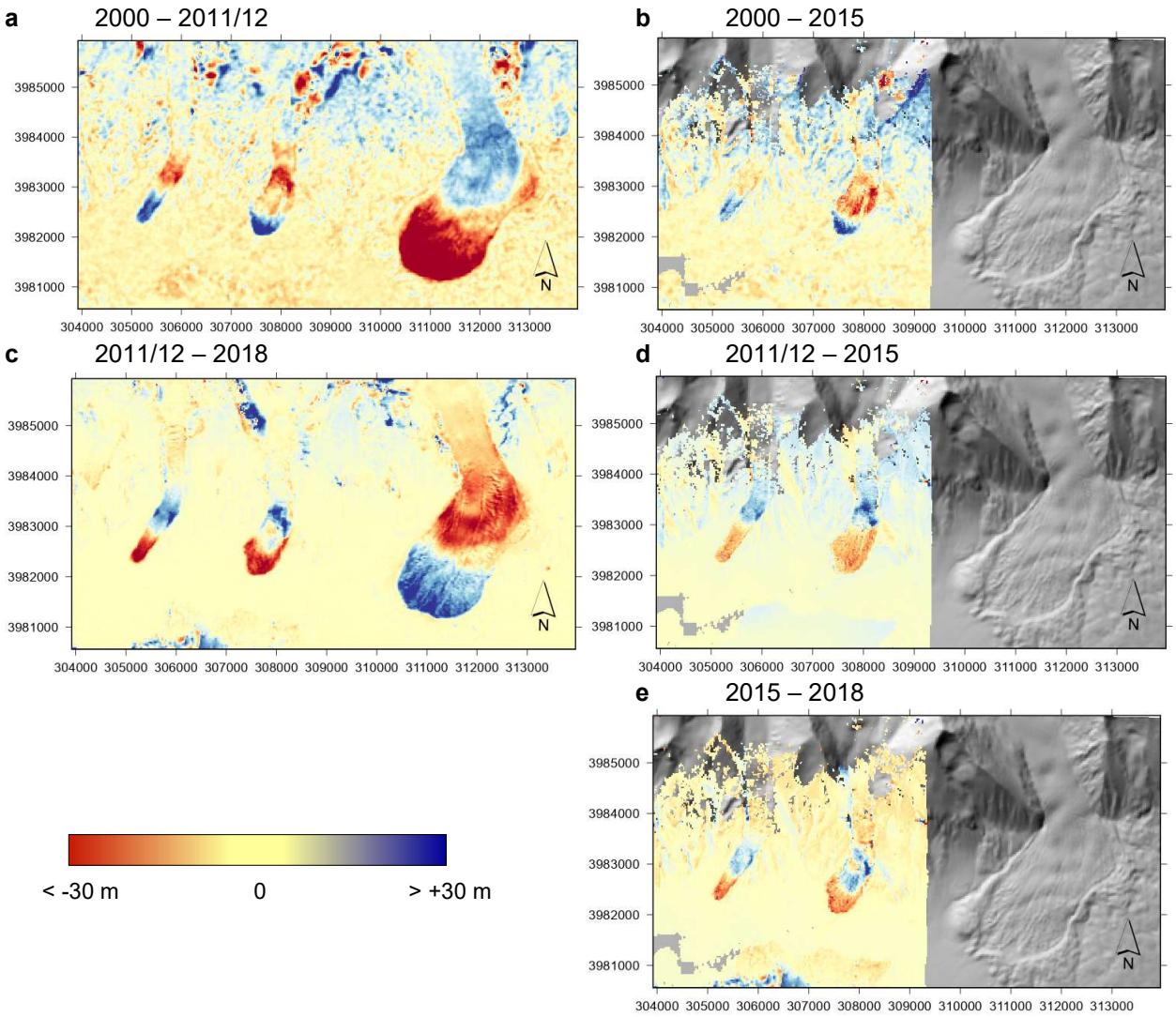

Fig. S11. Digital elevation model differences.

Bukadaban West glacier to the left, Bukadaban East glacier to the middle, and Zu Glacier to the right for reference. **a**, Elevation differences between the SRTM elevation model of 2000 and the Copernicus DEM with elevations from 2011/12. Blue shades are elevation increases, red shades are elevation losses. Saturation at ±30 m, see legend at bottom. UTM zone 46 coordinates. **b**, Elevation differences between the SRTM elevation model of 2000 and a HMA single DEM of 2015. The HMA DEM used here does not cover the entire section. Copernicus DEM hillshade in the background. **c**, Elevation differences between 2011/12 and 2018 TanDEM-X data. TanDEM-X change product © DLR 2024 (*36*). **d**, Elevation differences between the Copernicus DEM with data from 2022/12 and a HMA single DEM of 2015. **e**, Difference between data of panels **c** and **d**, i.e. elevation differences between 2015 and 2018, indicate a mass bulge travelling down the tongues of Bukadaban West and East glaciers.

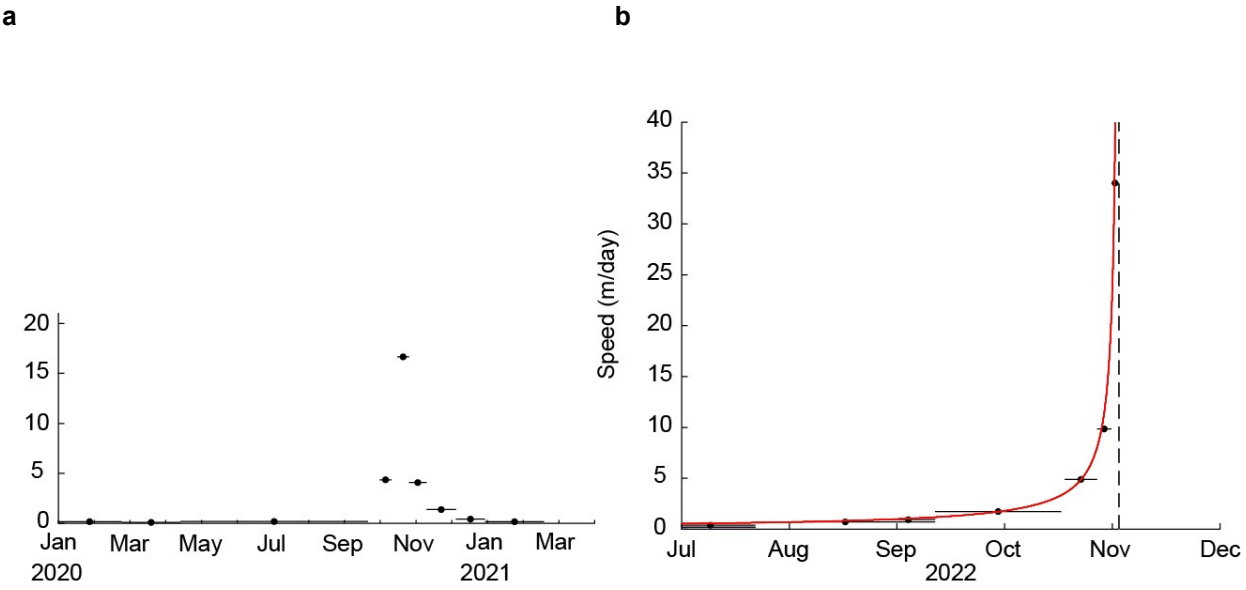

Fig. S12. Ice speeds.

Average ice speeds over time for a zone in the middle of the glacier tongues. X-axis: months, y-axis speed in m/day. Horizontal bars indicate the measurement periods. **a**, Bukadaban West. **b**, Bukadaban East, with a power law function fitted [4] (red). The vertical dashed line is the detachment date, 1 Nov 2022. Note, the time scale (x-axis) is different between the two panels.

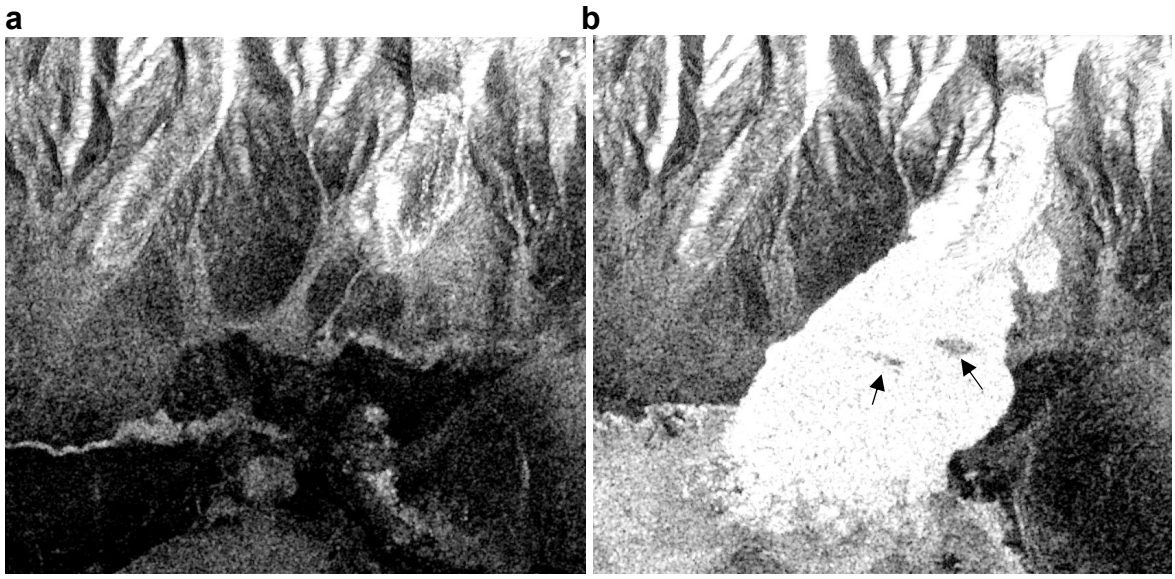

Fig. S13. Satellite radar images.

Sentinel-1 satellite radar images of (**a**) 26. Oct and (**b**) 2. November 2022, approx. 30 hours after detachment, show no signs of wet ice debris around the glacier tongue (**a**) and on the avalanche surface (**b**). The radar backscatter amplitude is a function of competing influences, in particular surface roughness (rough glacier surfaces show enhanced backscatter) and surface wetness (wet surfaces show decreased backscatter). While high backscatter is expected over the rough avalanche debris, wet conditions would still reduce radar backscatter and could thus produce darker grayscales, as for instance in the middle of the avalanche surface due to ice melt above the warm springs (arrows). The glacier detachment area has a smooth surface so that the backscatter influence from surface roughness should be limited, and a wet surface would likely produce less backscatter than observed. (Images downloaded from Copernicus Browser).